Collective excitations and inelastic electron scattering in semiconductor superlattices

Xiaoju Wu and Sergio E. Ulloa
Department of Physics and Astronomy and Condensed Matter and Surface Sciences Program, Ohio University, Athens, Ohio, 45701-2979
(Received 10 June 1993)

We present a theoretical investigation of the collective excitations in doped tunneling semiconductor superlattices by calculating the loss functions describing inelastic electron scattering and Raman scattering experiments. The dynamical response of this inhomogeneous electron system is treated within the random-phase approximation. Our calculations indicate that in addition to the conventional plasma modes associated with the in-phase motion of all electrons in the system, as well as the single-particle-like transitions with nonvanishing oscillator strength, there exist plasma modes related with the charge depletion in the surface layers of typical systems. A tunneling plasma mode corresponding to the electron motion along the superlattice growth direction is also shown to exist. The dispersion relations for the different plasma modes are obtained together with their effective oscillator strength for both inelastic electron and light scattering experiments. The strongest intraminiband plasmon behaves like that in two-dimensional electron systems in the small $q_{\|}$ regime, while the surface plasma modes exhibit an acousticlike linear dispersion due to the screening of the electrons in the bulk subbands. The behavior of the tunneling plasma mode is intermediate to these two. We show explicitly that the two experimental probes emphasize different modes in the various wave-vector regimes, and are therefore rather complementary.

I. INTRODUCTION

Superlattices are an interesting class of materials composed of alternating thin layers of two or more different constituents. As a first approximation, superlattices represent an ideal and periodic band modulation along the growth direction. The resulting one-dimensional potential well chain affects the motion of the electrons in the growth direction so that the conduction band is effectively split into a series of subbands or minibands.[1] Each of these subbands represents a continuum of free-electron-like states in the plane perpendicular to the growth direction, producing an interesting anisotropic three-dimensional (3D) electronic system. On the other hand, finite length superlattices with only a few periods along the growth direction have also been fabricated where superlattice surface states are created near the end layers, due to the existence of surface dangling bonds, as well as defects and impurities which pin the Fermi level. The Fermi level pinning produces a position-dependent density profile of charge carriers, depleting them from the end layers even in the case of homogeneous doping. All of these systems have received considerable attention because of their technological interest and also because of the fundamental physics involved.[1,2]

In this work, we focus on the electronic modes characteristic of these systems. There are numerous theoretical papers studying collective excitations in superlattices.[3–7] However, previous work has not considered all the intricacies mentioned above and found in real structures. One can trace the various elements entering in the study of these anisotropic 3D systems, starting from the pioneering work of Chen, Chen, and Burstein,[8] who investigated the collective modes associated with the transitions between 2D subbands by using a relatively simple model. More complicated treatments of the intersubband transitions were first given by Dahl and Sham[9] and by Eguiluz and Maradudin.[10] As for electronic correlation effects, Vinter[11] and Ando[12] have stressed the importance of vertex corrections in 2D electron systems. Tselis and Quinn[13] gave a unified model of collective modes in inversion layers, while plasma modes for two-layer electron systems were discussed by Chin and co-workers.[14] The latter authors indicated that, in addition to the 2D plasmon, there exists an acoustical plasmon with a dispersion relation $\omega \sim q$ in a two-layer system. This linear dispersion relation typically arises in a system in which the electrons have different spatial extent. The acoustic plasmon can be viewed as an out-of-phase collective motion of electrons in one subband or state relative to the other. The polarization field for the electrons in one subband is strongly screened by the charge in the other one, producing a weaker restoring force and dispersion relation than the $\omega \sim \sqrt{q}$ relation in a pure 2D system.[2]

As for multilayer systems, such as multiple quantum wells where electrons cannot tunnel across, most authors viewed these systems as one-dimensional arrays of 2D electron gases, coupled only through their Coulomb interactions.[4,6] Tselis and Quinn[4] investigated collective excitations in an ideal superlattice system. In their theory, one can take into account higher order many-body effects, magnetic fields, and electron-phonon coupling.

Recently, electron-energy-loss spectroscopy (EELS) has been used extensively to study the collective excitations in nonuniform electron gases.[16] This technique is very sensitive to the dispersion of the collective modes

on the same scale of wavelength that characterizes the charge density profile at a semiconductor surface or at an interface between a semiconductor and another material. Namely, the electron-energy-loss method can explore the wave-vector regime $q_{\|}l \sim 1$, where l is the thickness of the spatial extension of the charge carrier in the surface or interface, and $q_{\|}$ is the in-plane momentum transfer of the scattered external electron.

On the other hand, inelastic light (Raman) scattering has also been used extensively to investigate the novel electronic structure and collective excitations in systems of highly reduced dimensionality.[17] Notice that the effective oscillator strength of the various excitation modes, especially those that are surface-related, is expected to be rather different in these two scattering processes, due to the different coupling mechanism, even as both processes provide the same information for the excitation energies. We explore further this point below as we compare explicit results for the systems under study and contrast their different characteristics.

Both EELS and Raman scattering experiments have stimulated many theoretical studies on the details of the scattering processes. For example, Ehlers and Mills[18] investigated the EELS yield from collective excitations in n-type semiconductors, with emphasis on the influence of the depletion and accumulation layers. Similarly, Yu and Hermanson have recently studied plasmons in accumulation layers of ZnO and InAs(110) (Ref. 19) with only two subbands populated and found that, also in these systems, there exists an acousticlike mode, in addition to the two-dimensional-like plasma mode.

In the pioneering work of Jain and Allen,[5] the inelastic light scattering intensities from a semi-infinite array of two-dimensional electron gas layers were calculated neglecting intersubband transitions, for simplicity. Hawrylak, Wu, and Quinn[6] have also calculated the Raman scattering intensities for finite quantum-well arrays, although also in the flat miniband approximation (without tunneling). Katayama and Ando[7] have also presented self-consistent calculations for the ground state and collective excitations of an infinite multiple-quantum-well system, in which the surface mode was not included and dispersion relations were not presented. Recently, we have also reported preliminary calculations of Raman yields for a superlattice system with both tunneling and charge depletion included.[20]

In this paper, we present a fully nonlocal description of collective excitations in doped tunneling semiconductor superlattices of finite size, such as $GaAs/Al_xGa_{1-x}As$, and focus on the calculations of the inelastic electron scattering intensity as a function of excitation energy and momentum transfer. These calculations augment the long wavelength results of Zhang, Ulloa, and Shaich, who used the d-parameter formalism to describe the optical response in similar systems.[15] Our results uncover a wealth of interesting mode behavior. We also present some of the main results for inelastic light scattering in order to compare how efficiently the different probes couple to the normal modes of the system. In the calculation, we incorporate fully the influence of the superlattice surface states mentioned above, allowing charge carrier tunneling among the different periods and depletion due to Fermi level pinning at the surfaces of the structure. In addition to the surface mode associated with charge depletion, and the usual 2D plasma mode, we obtain a novel tunneling mode due to carrier tunneling. As expected, the collective excitation energy and coupling to external probes of the different modes change in a rather complex fashion, as the wave vector changes. The scattering intensities for all the modes, especially those that are surface-related modes, are rather different in inelastic electron scattering and Raman scattering due to the different coupling matrix elements. We also comment on other differences between the two probes.

The outline of the remainder of the paper is as follows. In Sec. II, we present the model and basic formalism used in the calculation. The basic method for studying the response of the electron system is closely related to that discussed by Ehlers and Mills,[18] while we have extended it to suit our needs in the tunneling superlattice system. In Sec. III, we present our results and a detailed discussion on these and related issues.

II. FORMALISM

We consider a semiconductor superlattice as N quantum wells of width a separated by a series of potential barriers of thickness b and supported by a semi-infinite uniform medium of dielectric constant ϵ (see inset in Fig. 1). The period of the superlattice is $d = a + b$. The surface-parallel motion of the electron is treated as a free-electron gas characterized by an effective mass m. The lattice vibrations are ignored for now but their effects will be discussed in Sec. III. The ionized donors are assumed to be smeared out into a uniform positive background which just cancels the charge density generated by the free carriers. The electronic wave function $\Phi_n(z)$ and energy E_n of the tunneling motion along the z direction are calculated self-consistently, taking into consideration the carrier depletion produced by surface dangling bonds and impurities.[21] Therefore, the full wave function of a conduction electron can be written as

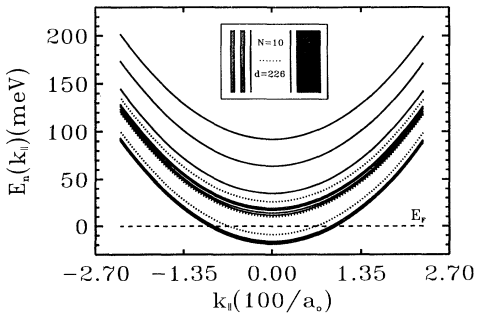

FIG. 1. Miniband structure for $GaAs/Al_xGa_{1-x}As$ superlattice of ten periods. Within a two-miniband model there are 20 levels, of which only the lowest five are occupied. The surface-related levels are shown as dotted lines. Inset shows a diagram of a superlattice used in the numerical calculation. d=226 Å and a_0 is the Bohr radius.

$$\Psi_{\mathbf{k}_\parallel,\mathbf{n}}(\mathbf{r}_\parallel,z)=\frac{1}{\sqrt{A}}\,e^{i\mathbf{k}_\parallel\cdot\mathbf{r}_\parallel}\,\Phi_n(z)\,, \tag{1}$$

and the corresponding eigenvalue is

$$E_n(\mathbf{k}_\parallel)=\frac{\hbar^2{k_\parallel}^2}{2m}+E_n\,, \tag{2}$$

where $\mathbf{r}_\parallel$,$\mathbf{k}_\parallel$ are position and wave vectors in the x-y plane.

The dynamical response of the inhomogeneous electron system is treated in a fully nonlocal theory within the random-phase approximation (RPA).[15] Correspondingly, the dielectric susceptibility χ describing the density-density correlation of electrons can be obtained by solving a Dyson equation:

$$\chi(\mathbf{q}_\parallel,\omega,z,z')=\chi_0(\mathbf{q}_\parallel,\omega,z,z')+\int_0^L\int_0^L dz_1\,dz_2\,[\,\chi_0(\mathbf{q}_\parallel,\omega,z,z_1)V(\mathbf{q}_\parallel,z_1,z_2)\,\chi(\mathbf{q}_\parallel,z_2,z')\,]\,, \tag{3}$$

where V is the Fourier component of the Coulomb interaction potential with Hartree and image terms given by

$$V(\mathbf{q}_\parallel,z,z')=V_H+V_I, \tag{4}$$

$$V_H=\frac{2\pi e^2}{\epsilon q_\parallel}\,e^{-q_\parallel|z-z'|}, \tag{5}$$

$$V_I=\frac{2\pi e^2}{\epsilon q_\parallel}\,\frac{\epsilon-1}{\epsilon+1}\,e^{-q_\parallel(z+z')}\,. \tag{6}$$

χ_0 is the susceptibility of the noninteracting electron system

$$\chi_0(\mathbf{q}_\parallel,\omega,z_1,z_2)=\sum_{n_1\,n_2}\Pi_{n_1\,n_2}\,\Phi_{n_1}(z_1)\Phi_{n_2}(z_1)\Phi_{n_1}(z_2)\Phi_{n_2}(z_2)\,, \tag{7}$$

where $\Pi_{n_1\,n_2}$ is given by

$$\Pi_{n_1\,n_2}=\sum_{\mathbf{k}_\parallel}\theta(E_F-E_{\mathbf{k}_\parallel\,n_1})\left[\frac{1}{\hbar\omega+E_{n_1}-E_{n_2}-\frac{\hbar^2}{2m}(2\mathbf{k}_\parallel\cdot\mathbf{q}_\parallel+q_\parallel^2)+i\eta}\right.$$
$$\left.-\frac{1}{\hbar\omega+E_{n_2}-E_{n_1}-\frac{\hbar^2}{2m}(2\mathbf{k}_\parallel\cdot\mathbf{q}_\parallel+q_\parallel^2)+i\eta}\right]. \tag{8}$$

A closed form of $\Pi_{n_1\,n_2}$ can be obtained through contour integration:[22]

$$\Pi_{n_1\,n_2}=-\frac{m^2}{\pi\hbar^4q_\parallel^2}\left\{2\left(\frac{\hbar^2q_\parallel^2}{2m^2}+\hbar\Omega_{n_2\,n_1}\right)+i\left[\frac{\hbar^4{q_\parallel}^2{k_F}^2}{m^2}-\left(\frac{\hbar^2{q_\parallel}^2}{2m^2}+\hbar\Omega_{n_2n_1}-\hbar\omega-i\eta\right)^2\right]^{1/2}\right.$$
$$\left.-i\left[\frac{\hbar^4{q_\parallel}^2k_F^2}{m^2}-\left(\frac{\hbar^2q_\parallel^2}{2m^2}+\hbar\Omega_{n_2n_1}+\hbar\omega+i\eta\right)^2\right]^{1/2}\right\}, \tag{9}$$

where $\hbar\Omega_{n_2\,n_1}=E_{n_2}-E_{n_1}$. The case $n_1=n_2$ corresponds to intrasubband transitions and $n_1\neq n_2$ describes intersubband transitions. The phenomenological damping parameter η is chosen to simulate typical impurity broadening of levels and is kept small in our numerical calculations below.

In a Wannier function representation, $\Phi_n(z)$ can be expressed as

$$\Phi_n(z)=\sum_{i,\alpha}b_{i\alpha}^n\,\phi_i^\alpha(z)\,, \tag{10}$$

where $\phi_i^\alpha(z)$ is the Wannier function for the αth miniband centered on the ith layer. Then, χ_0 can be written as

$$\chi_0(\mathbf{q}_\parallel,\omega,z,z')=\hat{\mathbf{A}}^t(z)\cdot\hat{\mathbf{B}}(\mathbf{q}_\parallel,\omega)\cdot\hat{\mathbf{A}}(z')\,, \tag{11}$$

where $\hat{\mathbf{A}}_s(z)=\phi_i{}^\alpha(z)\,\phi_j{}^\beta(z)$ and $\hat{\mathbf{B}}_{ss'}(\mathbf{q}_\parallel,\omega)=\sum_{nn'}b_{i\alpha}^nb_{j\beta}^{n'}\Pi_{nn'}b_{j'\alpha'}^nb_{j'\beta'}^{n'}$. Notice that $s=(\alpha,i,\beta,j)$ is a compound index.

The advantage of working in this Wannier representation is that the integral equation (3) can be decoupled and solved exactly.[9,23] We obtain

$$\chi(\mathbf{q}_\parallel,\omega,z,z')=\hat{\mathbf{A}}^t(z)\cdot\left[\hat{\mathbf{B}}(\mathbf{1}-\hat{\mathbf{V}}\hat{\mathbf{B}})^{-1}\right]\cdot\hat{\mathbf{A}}(z')\,, \tag{12}$$

where

$$\hat{\mathbf{V}}_{ss'}(\mathbf{q}_{\|}) = \int_0^L \int_0^L dz\, dz'\, \hat{\mathbf{A}}_s(z) V(\mathbf{q}_{\|}, z, z')\, \hat{\mathbf{A}}_{s'}(z')\,. \tag{13}$$

The definite-parity and the highly localized behavior of various ϕ_i^{α} greatly reduces the numerical calculation of the matrix elements $\hat{\mathbf{V}}_{ss'}$.[15]

An experimentally measurable quantity in both inelastic electron and light scattering experiments is the scattering cross section. This gives the probability for a process in which an incoming electron is "reflected" from a surface with a two-dimensional momentum transfer $\hbar\mathbf{q}_{\|}$ and energy loss $\hbar\omega$. It can be proved that the cross section at low temperature is proportional to the loss function:[24]

$$P(\mathbf{q}_{\|}, \omega) = \int_0^L P(\mathbf{q}_{\|}, \omega, z) dz\,, \tag{14}$$

where

$$P(\mathbf{q}_{\|}, \omega, z) = w^*(z) \int_0^L dz'\, w(z') \left[-\mathrm{Im}\chi(\mathbf{q}_{\|}, \omega, z, z')\right], \tag{15}$$

and

$$w(z) = \begin{cases} e^{-q_{\|}z} \text{ (inelastic electron scattering)} \\ e^{ik_z z} \text{ (inelastic light scattering),} \end{cases} \tag{16}$$

and $\mathrm{Im}\chi$ is the imaginary part of the susceptibility in Eq. (12). $P(\mathbf{q}_{\|}, \omega, z)$ describes the contribution to the total scattering intensity from different electron layers at position z and given $(\omega, \mathbf{q}_{\|})$, where k_z is the z component of wave vector of the incident light. Therefore, Eq. (14) sets up a relation between the microscopic nonlocal correlation function and an experimentally measurable quantity. Notice that the couplings between incoming beams (light and electron) and electrons in the superlattice are quite different. The electron beam couples via the rapidly decaying weight function in Eq. (16), while light is able to probe the whole structure. We would therefore expect different response intensities for the collective excitations in the two inelastic scattering experiments, as indeed we observe.

Finally, notice that all our calculations are in the RPA, so that the exchange-correlation effects are neglected. However, previous studies for similar superlattice systems by Katayama and Ando,[7] Zhang, Ulloa, and Schaich,[15] and others, have indicated that these terms do not affect significantly the energies of the collective modes and that the results obtained in the RPA agree extremely well with those of calculations that go beyond this approximation. This is of course a consequence of the nearly-three-dimensional character of electrons in these superlattices, and is in contrast to the situation in purely 2D systems, where higher order corrections are indeed essential.[25,26]

III. RESULTS AND DISCUSSIONS

Using the expressions derived in the preceding section, we have calculated the loss functions $P(q_{\|}, \omega)$ for an n-type doped semiconductor superlattice with typical structure parameters. The superlattice structure considered in our sample calculation consists of ten periods deposited on an undoped semi-infinite dielectric subtract, as shown in the inset of Fig. 1. In the typical $GaAs/Al_xGa_{1-x}As$ superlattice we model, the effective electron mass is $m = 0.067$ and the dielectric constant is $\epsilon = 12.5$. The period of the superlattice and the doping density are taken to be d=188(well) Å+38(barrier) Å= 226 Å and $\rho = 1.9\times10^{17}$ cm^{-3}, respectively. In addition, a two-miniband model is adopted and twenty subbands are involved in the calculations, which imposes significant demands on the CPU time invested in the calculation and inversion of matrices in Eq. (12). The broadening parameter η is taken to be 0.5 meV in the calculation. The self-consistent ground state energy-level structure and wave functions for the superlattice considered were obtained using a tight-binding envelope-function method developed by Zhang and co-workers.[21] In this method, the potential associated with the inhomogeneous charge-depletion layers is incorporated self-consistently. The termination of the finite superlattice gives rise to near surface-localized states lying in the miniband gap and with wave functions strongly peaked near the end layers of the superlattice, and with a fast-decaying tail of one unit period typically. Figure 1 shows the resulting level structure for our example, including surface-related subbands. The surface-localized states (dotted lines) lie close to the Fermi level and are detached from the main group of levels. In the discussion of the collective excitations of these superlattices with depletion layers, the surface states play an important role.

Notice that the collective excitations examined by Zhang, Ulloa, and Schaich[15] are the modes with oscillations in the direction perpendicular to the surface, and no momentum transfer from the probe is allowed in this long wavelength limit. All these modes can, of course, be described as vertical transitions between different subbands in terms of electronic levels, as supported by the nonzero excitation energies in the long wavelength limit. Nevertheless, the response undergoes rather important changes as the wave vector leaves the long wavelength regime, as electrons with different spatial positions cease to respond in phase to the external probes. From this also, one can expect that the effects of charge depletion and carrier tunneling in the superlattice would then influence the dispersion and coupling strength of the plasma modes. Given the complex nature of this problem, detailed numerical work is necessary to investigate this behavior, as we show below.

We turn our attention to the dynamical response of the systems considered. Figure 2 gives the loss function $P(q_{\|}, \omega)$ versus ω for different wave vector $q_{\|}$, for the inelastic *electron* scattering process. For convenience, all 2D wave vectors are presented in units of $q_0 = 2\pi \times 10^{-3}$ Å^{-1}. For comparison, the loss function for inelastic *light* scattering is also shown in Fig. 3 for several wave vectors. Moreover, we also present in Fig. 4 the loss function for an *ideal* periodic superlattice (no depletion regions) with the same structure parameters and doping density. To help identify the nature of the collective modes in

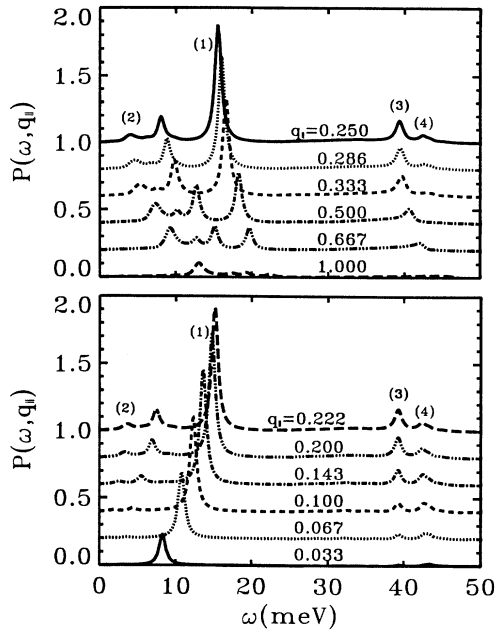

FIG. 2. Inelastic *electron* scattering intensities for different parallel momentum transfer values (in units of $q_0 = 2\pi \times 10^{-3}$ Å^{-1}). Each curve is displaced vertically for clarity. Intensity is in arbitrary units. Peaks (1) and (2) are numbered according to Fig. 7.

the nonuniform electron systems, the position-dependent loss function $P(q_{\|}, \omega, z)$ is also presented in Figs. 5 and 6 for the inelastic electron scattering and Raman scattering, respectively. The various collective excitations can be classified into two categories: intraminiband modes ($\hbar\omega \leq 30$ meV) and interminiband modes ($\hbar\omega \geq 30$ meV). Figure 7 gives the intensity (peak height) for several prominent modes as a function of $q_{\|}$ for the electron scattering probe. The corresponding oscillator strengths for the same modes in Raman scattering are also presented in the inset of Fig. 7 for the purpose of comparison. The dispersion relations are shown in Fig. 8. Each set of modes will be discussed next in detail.

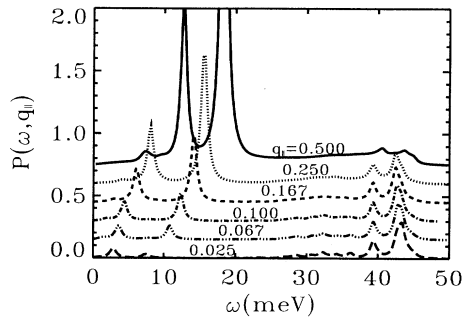

FIG. 3. Inelastic *light* scattering intensities for parallel momentum transfer values (in units of $q_0 = 2\pi \times 10^{-3}$ Å^{-1}). Each curve is displaced vertically for clarity. Intensity is in arbitrary units. Notice considerable differences in relative mode intensities with Fig. 2.

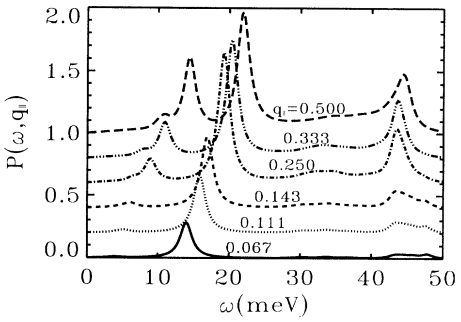

FIG. 4. Inelastic *electron* scattering intensities of an ideal periodic superlattice for various parallel momentum transfer values (in units of $q_0 = 2\pi \times 10^{-3}$ Å^{-1}). Each curve is displaced vertically for clarity. Intensity is in arbitrary units.

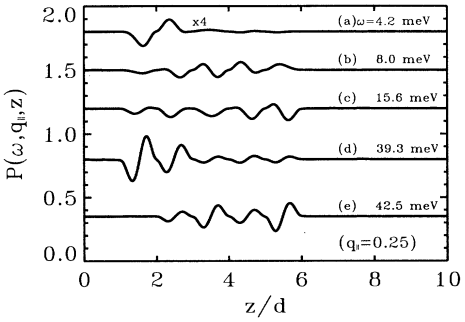

FIG. 5. Inelastic *electron* scattering amplitudes from a different electron z layer along the superlattice growth direction for $q_{\|} = 0.25q_0$. Each curve corresponds to a different frequency mode as indicated. Intensity is shown in arbitrary units.

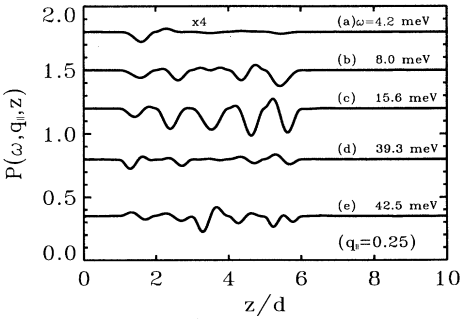

FIG. 6. Inelastic *light* scattering amplitudes from a different electron z layer along the superlattice growth direction for $q_{\|} = 0.25q_0$. Each curve corresponds to a different frequency mode as indicated. Intensity is shown in arbitrary units.

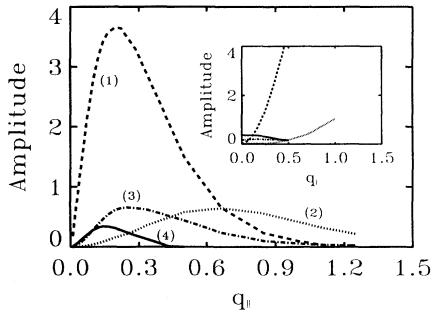

FIG. 7. Inelastic *electron* scattering amplitudes in arbitrary units as a function of wave vector for different plasma modes as indicated. Inset shows the inelastic light scattering amplitudes in arbitrary units as a function of wave vector; notice different decay behavior, produced here only by Landau damping. Curves (1) and (2) are for the main "bulk" plasma mode and surface mode, respectively. Curves (3) and (4) are for the two interminiband modes.

A. Intraminiband plasma modes

All intraminiband plasma modes are associated with collective motion (transitions) within each populated subband or between the partially occupied subbands. The loss functions in Fig. 2 indicate that all the prominent intraminiband modes appear well below $\hbar\omega$=30 meV in this structure. In this range, and for $q_\parallel \geq 0.25$, there exist four distinct modes in the electron scattering calculation (Fig. 2). As $q_\parallel$ decreases to $q_\parallel = 0.25$, the mode with the second highest frequency disappears. If $q_\parallel$ is further decreased to 0.05, there is only one mode left in the loss function curve and all others are too weak to be observed. The dispersion in Fig. 8 and oscillator strength curves in Fig. 7 indicate that these collective modes have rather rich structures as $q_\parallel$ goes from the long wavelength limit to the finite region. Comparing

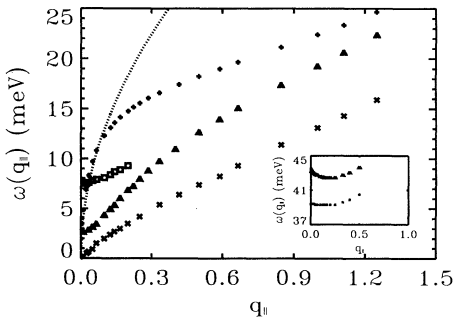

FIG. 8. Dispersion relations for different modes in Fig. 2. Intraminiband plasma modes: surface [×, peak (1) in Fig. 2], tunneling (△), and bulk [+, peak (2) in Fig. 2] modes. □ curve is the collective mode related to surface-to-miniband transitions. Interminiband modes are shown in the inset. Low (high) energy curve is the surface-related (bulk) mode. Upper dashed line shows the dispersion for a 2D plasmon, for comparison.

the loss function of the ideal superlattice (Fig. 4) with those of the superlattice of finite size (Fig. 2), we conclude that, except for the first peak (mode), there exists a one-to-one correspondence between the plasma modes in these two different systems. This suggests that the lowest energy peak in the loss function of the real superlattice [labeled (2) in Fig. 2] is associated with the collective excitations in the depletion layer, while other peaks correspond to "bulk" plasma modes. This result is also supported by the fact that this surface mode has dominant oscillator strength in the large $q_\parallel$ regime [Fig. 2 and curve (2) in Fig. 7]. More convincing evidence for this point is the behavior of the z-dependent loss function shown in Figs. 5 and 6, in which $P(q_\parallel, \omega, z)$ at $q_\parallel = 0.25$ is plotted for various modes. Curves (a), (b), and (c) correspond to three prominent intraminiband modes with excitation energy of 4.2, 8.0, and 15.6 meV, respectively. Clearly, the first mode is strongly localized in a few surface layers. Notice that this surface mode exhibits an acousticlike dispersion relation (× curve in Fig. 8) and has a zero excitation energy as the wave vector goes to zero. The 2D-like weak Coulomb potential in the surface layers is responsible for the vanishing frequency in the long wavelength limit. The surface mode can be viewed classically as the out-of-phase motion of the electrons in the surface layers with respect to the bulk layers. Accordingly, the polarization field in the surface layers is strongly screened by the electrons in the bulk layers (the electrons in the low-lying subbands), which produces the linear dispersion. A similar acousticlike mode has also been found in ZnO and InAs(110) systems[19] with accumulation layers and other quantum-well systems.

The main peak in Fig. 2 [labeled (1)] carries most of the intensity as the wave vector enters the $q_\parallel \leq 0.5$ region, and corresponds to the in-phase motion of all electrons including those in the depletion region. For even smaller wave vectors ($q_\parallel \leq 0.1$), which corresponds to a length equal to five times the total length of the superlattice, the dispersion relation (+ curve in Fig. 8) agrees very well with that of the ideal two-dimensional electron gas: $\omega(q_\parallel) = [2\pi n e^2 q_\parallel/\epsilon m]^{1/2}$. This implies that, when $q_\parallel \leq 0.1$, the nonuniform electron system behaves effectively as an ideal two-dimensional electron gas with all its carriers oscillating in phase. On the other hand, the dispersion curve for the 2D-like plasma mode departs increasingly from that of the ideal 2D electron gas as expected, due to the internal electronic structure of the superlattice. This mode also exhibits a vanishing frequency in the long wavelength limit. In this limit, all the electrons in the system respond to the external perturbation in phase, even though the equilibrium density is not homogeneous and the superlattice has finite thickness. Incidentally, notice that the general dispersion relations of the plasma modes obtained in inelastic electron scattering and Raman scattering are the same, although the oscillator strengths are quite different.

Curves (1) and (2) in Fig. 7 are the electron scattering oscillator strengths as a function of wave vector $q_\parallel$ for the main bulk mode and the surface mode. These two modes have roughly the same strength around $q_\parallel = 0.65$. While the bulk mode carries a very small portion of the intensity

due to the strong damping of the field, the surface mode dominates in strength in the large wave-vector regime ($q_{\|} \geq 0.65$). This implies that the surface-related modes would be more easily observed in the large wave-vector region in the inelastic electron scattering than in Raman scattering. Moreover, in the intermediate regime of the wave vector, both modes carry a substantial part of the total intensity. In contrast, as the wave vector goes to the regime below 0.3, where the damping of the probing field is relatively weak, the bulk mode has the largest oscillator strength as expected, since only a very small portion of the total number of electrons is in the surface layers. Meanwhile, as the wave vector goes to $q_{\|} \geq 0.5$, all the peaks in Fig. 2 become weak and broad, which can be understood in terms of the interaction between the plasmon and single-particle excitations (Landau damping).

The second peak in the loss function curves is called a *tunneling* mode, as it is associated with the tunneling motion of electrons along the superlattice growth direction. This novel mode has a nonzero excitation energy of 2.8 meV as $q_{\|} \to 0$ ($\triangle$ curve in Fig. 8). This energy can be viewed as arising from transitions among the bulk-related subbands of the structure but shifted by the Coulomb interaction from 2.6 meV (Fig. 1). Curve (c) in Figs. 5 and 6 indicates that the tunneling mode is basically extended throughout the superlattice. As far as the oscillator strength is concerned, our calculations show that the collective tunneling mode carries substantial intensity if the wave vector is within the region 0.1–1. Again, this mode enters the Landau damping region and becomes not well-defined as the wave vector increases beyond 1.3. The d-parameter theory of Zhang, Ulloa, and Schaich[15] obtained similar results for the same system in the long wavelength regime.

Notice in Fig. 2 that there exists another mode with excitation energy intermediate to the tunneling mode and the surface mode in the inelastic electron scattering as the wave vector goes beyond 0.25. Our calculation shows that both the excitation energy and oscillator strength vanish as the wave vector approaches zero and are always small (the dispersion is not included in Fig. 8). This mode is identified as a mixed result of all possible coherent motions of the electrons in different layers. In terms of electronic levels, there should exist many possible coherent transitions among the populated subbands, and indeed this mode carries its highest intensity for large wave vectors on and around 0.7, but eventually it Landau dampens for values close to 1.

Before ending the discussion of the intraminiband collective excitations, a comparison between the inelastic electron and light scattering results is necessary. As mentioned before, due to the different coupling mechanism in these two scattering processes, there exists rather prominent differences in the intensity curves for the surface-related modes. For large wave vectors, the surface modes dominate in effective oscillator strength in the inelastic electron scattering, while this characteristic is absent in the Raman scattering. Given the same wave vector of 0.25 in Figs. 5 and 6, $P(q_{\|}, \omega, z)$ for the surface mode in these scattering processes is plotted [curve (a)]. Notice that the intensity in inelastic electron scattering is stronger than that in the Raman scattering, and even though both curves imply that this mode is strongly located around the surface layers, there are subtle differences that yield different total amplitudes. This important point is even more clear for the surface-related interminiband mode, which will be discussed next. Indeed, surface-related modes would be preferentially enhanced in inelastic electron scattering compared with the results of Raman scattering experiments.

B. Interminiband plasma modes

As Figs. 2 and 3 indicate, in addition to the intraminiband plasma modes there also exist two interminiband plasma modes, associated with transitions across the miniband gap. The corresponding dispersion and oscillator strength are also given in Fig. 8 (inset) and Fig. 7, respectively. Between the interminiband and the intraminiband energies there is a large single-particle-like excitation continuum in which no plasma mode can exist. Moreover, the single-particle excitations also exist in other energy regions with small but nonvanishing strength. For small wave vector $q_{\|}$, the energy gap between the single-particle excitations and plasmons forbids the exchange of their energy. The gap will decrease and eventually vanish as $q_{\|}$ increases and the system then enters the strong Landau damping regime.

In a simple case, for example, when only two subbands are involved in the calculation and the effect of other subbands can be neglected due to a large energy separation, the interminiband plasma resonance can be viewed as coming from the corresponding single-particle transition but shifted by the depolarization fields.[8,9] The energy shift in the long wavelength approximation is proportional to the volume charge density n and a Coulomb integral f such that $\omega(q_{\|}) = \sqrt{\omega_e^2 + f\omega_p^2}$, where ω_e is the separation of the two subbands considered, and ω_p is the well-known plasma frequency of the equivalent 3D system. When more subbands are included, as in the case of the tunneling superlattice considered in this paper, and the included subbands have very close energy values to form a miniband, the complicated and stronger polarization fields will also cause significant shifts in the excitation spectrum.[9] Several empty subbands with energies lying close to the occupied states have an important contribution to yield a large mode strength. The spatial dependent loss function shown in curve (d) of Figs. 5 and 6 confirms that the first interminiband plasma mode [labeled (3) in Fig. 2] is mainly confined to the end layers, while the higher energy mode is basically extended throughout the superlattice. This also agrees with its absence in Fig. 4, as the ideal superlattice supports no surface states or modes, and it only shows one broad interminiband mode. We therefore conclude that the first interminiband mode corresponds to the transitions from the populated surface subband to the unoccupied bulk-like subbands. In contrast, the second mode [(4) in Fig. 2] describes the tunneling among the different wells and basically results from transitions from the lowest four extended occupied subbands to the empty subbands. The

oscillator strength curves as a function of wave vector for these two modes in the inelastic electron scattering, represented by curves (3) and (4) in Fig. 7, show that mode (4) decays fast to zero as the wave vector increases from 0.15 to 0.45, while mode (3) exhibits a very slowly decaying behavior and reaches zero only after 1.25. The rapid intensity decay of the second mode can be attributed to the factor $e^{-q_{\|}z}$ in the bulk region (z very large) in Eq. (16). On the other hand, the decay of the first mode at large $q_{\|}$ is mainly due to the Landau damping.

The dispersion curve for the first mode remains almost constant at about 39.4 meV when $q_{\|} \leq 0.286$. In the small $q_{\|}$ regime, the depolarization field of the induced charge density fluctuation parallel to the surface in the depletion layer appears to change very slowly, and produces no mode dispersion. The situation is different, however, as the excitation energy increases for wave vectors beyond 0.286. In contrast, the dispersion of mode (4) exhibits a negative slope in the small wave-vector region, changes into a positive slope at $q_{\|}$=0.15, and eventually the mode disappears at 0.45. This somewhat unusual negative slope behavior in the interminiband dispersion relation has been found in other systems as well.[22] Moreover, as discussed before, optical absorption calculations[15] also obtained two interminiband plasma modes with excitation energies of 39.8 and 42.5 meV, respectively, which agree with our results of 39.4 and 42.4 meV in the long wavelength limit.

Before concluding this part of the discussion, we would like to comment on the effect of phonons in our calculations. We have treated the dielectric response of electrons in the tunneling superlattice without including the contribution of the lattice vibrations. Generally speaking, polar semiconductors have an infrared-active transverse optical phonon mode at long wavelength. This mode usually plays an important role in inelastic electron scattering. Therefore, in order to compare with experimental results, in principle, one needs to incorporate the effect of the lattice vibrations. This can be done by replacing the frequency-independent dielectric constant by a frequency-dependent dielectric function: $\epsilon(\omega) = \epsilon_{\infty}(\omega^2 - \omega_L^2 + i\eta_{\rm ph}\omega)/(\omega^2 - \omega_T^2 + i\eta_{\rm ph}\omega)$. For GaAs, $\hbar\omega_T = 33.6$ meV and $\hbar\omega_L = 36.8$ meV, and $\eta_{\rm ph}$ is a phenomenological parameter for phonon broadening. When phonons are included in the dielectric response calculation, and because of the interaction of the polarization fields of phonon and plasmon, new coupled modes arise. These new modes are basically a mixture of the plasma and phonon modes. However, this coupling has a substantial influence only when the energy difference of these two modes is small. Therefore, in case of a large energy difference, only one extra phononlike mode will be obtained as the original modes would have only a slight shift to higher energy when the lattice vibration is incorporated in the picture. Since for GaAs $\hbar\omega_T$ is rather far from both the main intraminiband peak and the first interminiband mode for all wave vectors of interest, we do not expect to obtain qualitative differences, except around the phonon absorption peak $\hbar\omega_T = 33.6$ meV.

IV. SUMMARY

We have applied a full nonlocal response theory in a Wannier function representation to study the collective excitations and their dispersion relations by calculating the loss function describing the inelastic electron-electron scattering and Raman scattering experiments for doped tunneling semiconductor superlattices such as $GaAs/Al_xGa_{1-x}As$ with charge depletion in the surface layers. In the calculation, a total of twenty subbands are involved, out of which only five subbands are occupied. This work complements the results obtained by Zhang, Ulloa, and Schaich[15] for a similar superlattice system, providing detailed information for mode intensity and dispersion relation, well beyond the long wavelength regime. The complicated depolarization fields, which are created by the electrons in different subbands, govern the dispersion relations of different modes. All the intraminiband modes describe the collective motion parallel to the surface, while the interminiband plasmons are associated with a small polarization along the superlattice growth direction. As $q_{\|}$ goes to zero, these two kinds of modes have vanishing and nonvanishing excitation energy, respectively. The novel tunneling mode has nonzero frequency in the long wavelength limit. Especially, the surface-related intraminiband mode has an acousticlike dispersion curve, which can be attributed to the screening of the electrons in the bulk layer. Besides, for small wave vectors, the dominant intraminiband mode exhibits a very strong 2D-like electron gas behavior. On the other hand, the mode exhibits substantially different responses to the two external probes studied here. This produces different mode intensities in the loss function due to the unique coupling process. The fast decay of the oscillator strength in EELS for the bulk-related modes in the large $q_{\|}$ regime is mainly due to the damping factor $e^{-q_{\|}z}$. However, the intensity of the surface-related modes results from Landau damping. The inelastic electron and light scattering complement each other well in that the inelastic electron scattering is more sensitive to the surface-related normal modes. We are hopeful that this work will encourage comparative studies on the same superlattice structure as a way to characterize all modes of the structure well.

ACKNOWLEDGMENTS

We express our thanks to W. L. Schaich for extensive discussions and encouragement during this work. Calculations were performed on the Cray Y/MP at the Ohio Supercomputer Center under Project PHS060. This project was supported by the U.S. Department of Energy, Grant No. DE-FG02-91ER45334.

[1]P. J. Stiles, in *Interfaces, Quantum Wells and Superlattices,* Vol. 179 of *NATO Advanced Study Institute, Series B: Physics*, edited by C. R. Leavens and R. Taylor (Plenum, New York, 1988).
[2]T. Ando, A. B. Fowler, and F. Stern, Rev. Mod. Phys. **54**, 437 (1982).
[3]S. Das Sarma and J. J. Quinn, Phys. Rev. B **25**, 7603 (1982); S. Das Sarma, *ibid.* **29**, 2334 (1984); R. D. King-Smith and J. C. Inkson, *ibid.* **33**, 5489 (1986); J. K. Jain and S. Das Sarma, *ibid.* **35**, 918 (1987); G. Eliasson, P. Hawrylak, and J. J. Quinn, *ibid.* **35**, 5569 (1987); W. Que and G. Kirczenow, *ibid.* **36**, 6596 (1987); G. F. Giuliani, P. Hawrylak, and J. J. Quinn, Phys. Scr. **36**, 946 (1987); X. Zhu, X. Xia, J. J. Quinn, and P. Hawrylak, Phys. Rev. B **38**, 5617 (1988).
[4]A. C. Tselis and J. J. Quinn, Phys. Rev. B **29**, 3318 (1984).
[5]J. K. Jain and P. B. Allen, Phys. Rev. Lett. **54**, 947 (1985); **54**, 2437 (1985); Phys. Rev. B **32**, 997 (1985).
[6]P. Hawrylak, J. W. Wu, and J. J. Quinn, Phys. Rev. B **32**, 5169 (1985).
[7]S. Katayama and T. Ando, J. Phys. Soc. Jpn. **54**, 1615 (1985).
[8]W. P. Chen, Y. J. Chen, and E. Burstein, Surf. Sci. **58**, 263 (1976).
[9]D. Dahl and L. J. Sham, Phys. Rev. B **16**, 651 (1977).
[10]A. Eguiluz and A. A. Maradudin, Ann. Phys. (N.Y.) **29**, 1113 (1978).
[11]B. Vinter, Phys. Rev. B **13**, 4447 (1976); **15**, 3947 (1977).
[12]T. Ando, Z. Phys. B **26**, 263 (1977).
[13]T. Tselis and J. J. Quinn, Surf. Sci. **113**, 362 (1982).
[14]K. W. Chin, J. J. Quinn, T. K. Lee, and A. Eguiluz, Phys. Rev. B **11**, 4989 (1977); S. Das Sarma and A. Madhukar, *ibid.* **23**, 805 (1981).
[15]J. Zhang, S. E. Ulloa, and W. L. Schaich, Phys. Rev. B **41**, 5467 (1990); **43**, 9865 (1991).
[16]U. Backes and H. Ibach, Solid State Commun. **40**, 575 (1981); U. Backes and H. Ibach, *ibid.* **48**, 445 (1983); S. A. Lindgren and L. Walldén, Solid State Commun. **25**, 13 (1980); Phys. Rev. B **22**, 5967 (1980); P. Soukiassian, R. Riwan, and Y. Borensztein, Solid State Commun. **44**, 1375 (1982); P. Soukiassian, R. Riwan, C. Guillot, J. Lecante, and Y. Borensztein, Phys. Scr. **T4**, 110 (1983); F. J. Crowne, Phys. Rev. B **27**, 3201 (1983); B. N. J. Person and J. E. Demuth, *ibid.* **30**, 5968 (1984); L. H. Dubois, G. P. Schwartz, R. E. Camley, and D. L. Mills, *ibid.* **29**, 3208 (1984).
[17]A. Pinczuk, S. Schmitt-Rink, G. Danan, J. P. Valladares, L. N. Pfeiffer, and K. W. West, Phys. Rev. Lett. **63**, 1633 (1989); J. S. Weiner, D. Danan, A. Pinczuk, J. Valladares, L. N. Pfeiffer, and K. West, *ibid.* **63**, 1641 (1989); A. R. Goñi, A. Pinczuk, J. S. Weiner, J. M. Calleja, B. S. Dennis, L. N. Pfeiffer, and K. W. West, *ibid.* **67**, 3298 (1991).
[18]D. H. Ehlers and D. L. Mills, Phys. Rev. B **36**, 1051 (1987); **34**, 3939 (1986).
[19]Hong Yu and J. C. Hermanson, Phys. Rev. B **41**, 5991 (1990); **40**, 851 (1989).
[20]Xiaoju Wu and S. E. Ulloa, Phys. Rev. B **47**, 6799 (1993).
[21]J. Zhang and S. E. Ulloa, Phys. Rev. B **38**, 2063 (1988); Solid State Commun. **71**, 643 (1989); Y. S. Joe and S. E. Ulloa, J. Phys. Condens. Matter **2**, 7137 (1990).
[22]L. Wendler and R. Pechstedt, Phys. Status Solidi B **138**, 197 (1986).
[23]C. H. Wu and W. Hanke, Solid State Commun. **23**, 829 (1977).
[24]H. Ibach and D. L. Mills, *Electron-Energy Loss Spectroscopy and Surface Vibrations* (Academic, San Francisco, 1982).
[25]D. Gammon, B. V. Shanabrook, J. C. Ryan, D. S. Katzer, and M. J. Yang , Phys. Rev. Lett. **68**, 1884 (1992).
[26]B. Jusserand, D. Richards, B. Etienne, H. Peric, and G. Fasol, Surf. Sci. **263**, 527 (1992).